A dynamic subgrid-scale model based on differential filters for LES of particle-laden turbulent flows

By George I. Park, J. Urzay, M. Bassenne AND P. Moin

1. Motivation and objectives

In Lagrangian descriptions of turbulent flows laden with heavy particles, the disperse phase is described by the equation of the trajectory

$$\frac{dx_{p,i}}{dt} = u_{p,i} \tag{1.1}$$

and the equation of motion

$$\frac{4}{3}\pi\rho_p a^3 \frac{du_{p,i}}{dt} = 6\pi\mu a(u_i - u_{p,i}), \tag{1.2}$$

where it is assumed that the flow around the particles is dominated by molecular transport. In this formulation, $x_{p,i}$ and $u_{p,i}$ are the particle position and particle velocity, ρ_p and a are the particle density and radius, and μ is the dynamic viscosity of the carrier phase.

In Eq. (1.2), u_i refers to the full-scale velocity of the carrier phase at the particle position, which in direct numerical simulations (DNS) is obtained by integrating the Navier Stokes equations. In contrast, in large-eddy simulations (LES) the only velocity available is the filtered one, denoted here by $\overline{u}_i$. In particular, when the mass of particles per unit mass of carrier phase is small, the filtered velocity is obtained by integrating

$$\frac{\partial \overline{u}_i}{\partial x_i} = 0 \tag{1.3}$$

and

$$\frac{\partial \overline{u}_i}{\partial t} + \overline{u}_j \frac{\partial \overline{u}_i}{\partial x_j} = -\frac{1}{\rho}\frac{\partial \overline{p}}{\partial x_i} + \nu \frac{\partial^2 \overline{u}_i}{\partial x_j \partial x_j} - \frac{\partial \mathcal{T}_{ij}^{\mathrm{DM}}}{\partial x_j}, \tag{1.4}$$

which represent, respectively, the filtered equations of mass and momentum conservation. In Eq. (1.4), $\overline{p}$ is the hydrodynamic pressure, ν is the kinematic viscosity, and ρ is the carrier-phase density, with $\rho/\rho_p \ll 1$ in most practical applications (Sánchez *et al.* 2015). The symbol $\mathcal{T}_{ij}^{\mathrm{DM}} = \overline{u_i u_j} - \overline{u}_i \overline{u}_j$ denotes the subgrid-scale (SGS) tensor, with the super-index DM used here to indicate that is computed using the dynamic Smagorinsky model of Germano *et al.* (1991). However, the model choice for $\mathcal{T}_{ij}$ is not essential to the description of the subgrid model for particles, as shown below.

The utilization of $\overline{u}_i$ in Eq. (1.2) in place of the full-scale velocity u_i leads to inaccurate results when the particles are sufficiently light to interact with SGS eddies. Expressed in dimensionless form, the critical condition that enables this interaction is (Urzay *et al.* 2014)

$$\mathrm{St}_{\mathrm{SGS}} = t_a/t_\Delta < 1, \tag{1.5}$$

where $\mathrm{St}_{\mathrm{SGS}}$ is an SGS Stokes number based on the characteristic particle-acceleration time $t_a \sim (2/9)(\rho_p/\rho)a^2/\nu$ and on the cutoff fluctuation time t_Δ induced by the eddies whose size is of the same order as the grid size Δ. In general, t_Δ is a time scale measured in the reference frame of the particle. In conditions where (1.5) is satisfied, the particles become tracers of the large eddies and the cutoff fluctuation time is given by Kolmogorov scaling $t_\Delta \sim (\Delta^2/\epsilon)^{1/3}$, where ϵ is the dissipation.

In this study, the focus is on LES of turbulent flows in which the particles interact with the unresolved eddies, $\mathrm{St}_{\mathrm{SGS}} < 1$. In this limit, unless an SGS particle model is employed to model the subgrid velocity fluctuations in Eq. (1.2), the effective maximum value of the Stokes number of the simulations based on small scales becomes that given by $\mathrm{St}_{\mathrm{SGS}}$. This value is, by definition, smaller than the Stokes number based on the subgrid scales, including that based on Kolmogorov scales. As a result, for the same set of parameters, LES renders smaller Stokes numbers in comparison with DNS. In LES, the deficit of subgrid scales has consequences on a number of metrics for the disperse phase such as relative dispersion, preferential concentration, turbophoresis and acceleration statistics.

The objective of this investigation is to formulate and test a model for the SGS velocity of the carrier phase to be used in conjunction with the filtered velocity $\overline{u}_i$ for integrating the particle equation of motion (1.2). The proposed model is based on differential filters (Germano 1986a,b) and employs a dynamic procedure to determine the value of an otherwise adjustable parameter. Using this model, LES of incompressible particle-laden homogeneous-isotropic turbulence are performed that show good agreement with DNS results in terms of relevant disperse-phase statistics, including preferential concentration.

This report is structured as follows. The formulation of the SGS model is described in Section 2. Numerical results of the model in LES of homogeneous-isotropic particle-laden turbulence are shown in Section 3, along with comparisons with DNS. Lastly, concluding remarks are provided in Section 4.

2. Formulation of the subgrid-scale model for the carrier-phase velocity

The SGS model for particles proposed here makes use of the elliptic differential filter to express the filtered velocity

$$\overline{u}_i(\mathbf{x},t) = \int_{\mathbf{x}'} u_i(\mathbf{x}',t) G(\mathbf{x},\mathbf{x}') d^3\mathbf{x}' \tag{2.1}$$

in terms of an exponentially decaying filter kernel

$$G(\mathbf{x},\mathbf{x}') = \frac{\exp\{-|\mathbf{x}-\mathbf{x}'|/b\}}{4\pi b^2 |\mathbf{x}-\mathbf{x}'|}. \tag{2.2}$$

In particular, G corresponds to the Green's function of the equation (Germano 1986a,b)

$$u_i = \overline{u}_i - b^2 \frac{\partial^2 \overline{u}_i}{\partial x_j \partial x_j}, \tag{2.3}$$

where b is a model parameter that controls the nominal filter width and is of the same order as the grid spacing Δ. Specifically, b is computed dynamically, as described below. In this formulation, bold symbols indicate vectors.

To apply the differential-filter-based model (DF), at each time step the carrier-phase de-filtered velocity u_i computed using (2.3) is employed in integrating the equation of motion for the particles (1.2). In the present one-way coupled simulations, the DF model

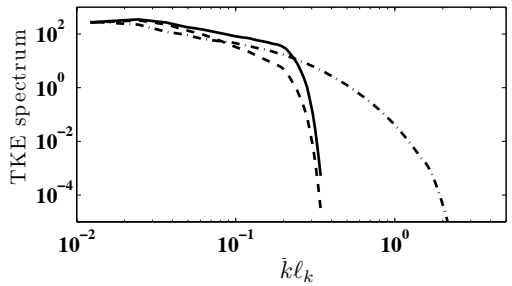

FIGURE 1. Turbulent kinetic-energy spectra in homogeneous-isotropic turbulence as a function of the wavenumber k, including DNS with 256^3 grid points (dot-dashed line), LES with 32^3 grid points (dashed line), and LES augmented with the SGS velocity computed using the dynamic DF model (2.4) in a 32^3 grid (solid line). Further details about the computational setup are provided in Section 3.

(2.3) is used only in the context of SGS particle modeling, and it is not involved in the integration of the carrier-phase conservation equations (1.3)-(1.4).

Note that the de-filtered velocity u_i computed using the DF model (2.3) has the same wavenumber range of spectral content as the resolved velocity $\overline{u}_i$, as shown in the numerical example in Figure 1. Similarly to other approximate deconvolution methods, the de-filtered velocity u_i does not involve scales smaller than the grid size. Therefore, u_i is not a full-scale quantity as in DNS, but rather is an intermediate velocity whose spectrum has been augmented by a subgrid velocity

$$u_i' = -b^2 \frac{\partial^2 \overline{u}_i}{\partial x_j \partial x_j}, \tag{2.4}$$

modeled as in a Faxén-like correction to account for the subgrid gradients. Contours of the DNS and LES velocities, along with the SGS velocity computed using Eq. (2.4) are shown in Figure 2, and correspond to the homogeneous-isotropic turbulent flow simulated in Section 3. In particular, the Fourier spectrum of the subgrid velocity u_i' vanishes at small wavenumbers while acting most intensely at wavenumbers of the same order as the grid cutoff. Remarkably, the numerical operation involved in computing u_i' from Eq. (2.4) (or u_i from Eq. (2.3)) can easily be done with any type of flow solver and grid, including unstructured setups. In a separate context of box filters, Eq. (2.3) resembles an approximate spatial de-averaging of the velocity u_i in which the Laplacian operator in the modeled fluctuations (2.4) is based on $\overline{u}_i$ instead of u_i in a first approximation of a series expansion in powers of Δ (Okong'o & Bellan 2000).

In contrast to stochastic models with adjustable parameterizations based on global quantities, the subgrid velocity model (2.4) contains explicit information from the LES resolved velocity field $\overline{u}_i$. Because of this characteristic, the subgrid velocity field takes into account localized hydrodynamic phenomena occurring in the resolved scales. However, an approximation has to be made in (2.3) that $\overline{u}_i$ is the implicitly filtered velocity computed from the LES, as opposed to being the differentially filtered velocity, although both quantities may not necessarily be the same. It is therefore not warranted that the closure (2.4) is consistent with, for instance, the model for the SGS stress tensor $\mathcal{T}_{ij}$ in Eq. (1.4). However, a suitable choice for the model parameter b in Eq. (2.3), which should not preferably make use of any adjustable parameters, can contribute to a higher degree

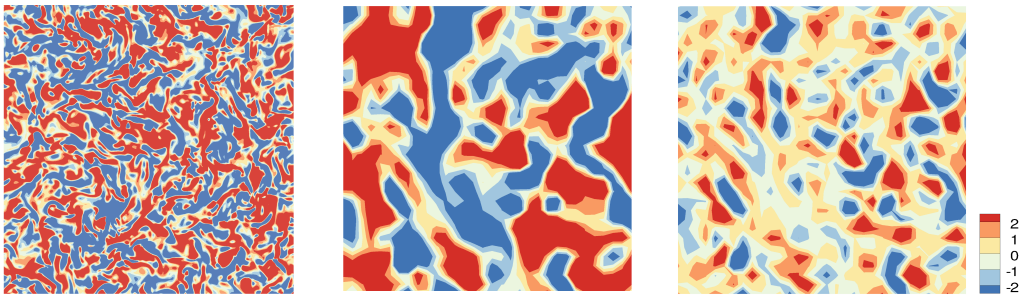

FIGURE 2. Contours of carrier-phase velocity in homogeneous-isotropic turbulence normalized with the integral velocity scale, including DNS in a 256^3 grid (left panel) and LES in a 32^3 grid (center panel). The figure also shows the SGS velocity contours computed using the dynamic DF model (2.4) normalized with the integral velocity scale in a 32^3 grid (right panel). Further details about the computational setup are provided in Section 3.

of consistency between the two. In particular, a dynamic procedure is presented below that is based on matching the SGS dissipation predicted by both models.

2.1. *Dynamic determination of the model parameter b based on SGS-dissipation consistency*

A dynamic procedure for computing model parameter b is used in this study that imposes consistency between the SGS dissipation calculated from the dynamic Smagorinsky model for the SGS stress tensor, $\epsilon_{\rm SGS}^{\rm DM} = -\mathcal{T}_{ij}^{\rm DM}\overline{S}_{ij}$, where $\overline{S}_{ij} = (1/2)(\partial\overline{u}_i/\partial x_j + \partial\overline{u}_j/\partial x_i)$ is the strain rate of the resolved velocity field, and the one obtained from the DF model for particles, $\epsilon_{\rm SGS}^{\rm DF} = -\mathcal{T}_{ij}^{\rm DF}\overline{S}_{ij}$, with $\mathcal{T}_{ij}^{\rm DF}$ an SGS stress tensor directly obtained from the differential-filter formulation, as explained below. Although dynamic procedures based on matching other quantities can easily be devised, this study focuses on matching just the SGS dissipation, since it is known that the correct prediction of the rate of transfer of energy from the resolved to SGS scales is a key factor in the successful performance of dynamic SGS models (Jiménez & Moser 2000).

The description of the dynamic procedure begins by deriving an expression of the SGS stress tensor $\mathcal{T}_{ij}^{\rm DF}$ based on making recursive use of the differential-filter definition (2.3) for computing

$$\overline{u_i u_j} = \overline{\left(\overline{u}_i - b^2\frac{\partial^2\overline{u}_i}{\partial x_k\partial x_k}\right)\left(\overline{u}_j - b^2\frac{\partial^2\overline{u}_j}{\partial x_m\partial x_m}\right)} \tag{2.5}$$

and

$$\overline{u}_i\overline{u}_j = \overline{\overline{u}_i\overline{u}_j} - b^2\frac{\partial^2}{\partial x_k\partial x_k}\overline{(\overline{u}_i\overline{u}_j)}, \tag{2.6}$$

which yields

$$\mathcal{T}_{ij}^{\rm DF} = \overline{u_i u_j} - \overline{u}_i\overline{u}_j = \overline{R}_{ij}, \tag{2.7}$$

where

$$R_{ij} = 2b^2\frac{\partial\overline{u}_i}{\partial x_\ell}\frac{\partial\overline{u}_j}{\partial x_\ell} + b^4\frac{\partial^2\overline{u}_i}{\partial x_k\partial x_k}\frac{\partial^2\overline{u}_j}{\partial x_m\partial x_m} \tag{2.8}$$

is an auxiliary tensor, with filtered velocities $\overline{u}_i$ being approximated as the LES resolved ones. In Eq. (2.7), the overbar in $\overline{R}_{ij}$ refers to the differential-filter operator acting on

R_{ij}. As a result, the differential-filter definition (2.3) applied to $\overline{R}_{ij}$, in conjunction with Eq. (2.7), lead to the relation

$$\mathcal{T}_{ij}^{\mathrm{DF}} = R_{ij} + b^2 \frac{\partial^2 \mathcal{T}_{ij}^{\mathrm{DF}}}{\partial x_k \partial x_k} \tag{2.9}$$

between R_{ij} and $\mathcal{T}_{ij}^{\mathrm{DF}}$.

The consistency condition between the SGS dissipations predicted by both models, $\epsilon_{\mathrm{SGS}}^{\mathrm{DF}} = \epsilon_{\mathrm{SGS}}^{\mathrm{DM}}$, can be expressed as

$$-\mathcal{T}_{ij}^{\mathrm{DF}} \bar{S}_{ij} = -\mathcal{T}_{ij}^{\mathrm{DM}} \bar{S}_{ij}, \tag{2.10}$$

with $\mathcal{T}_{ij}^{\mathrm{DM}}$ being calculated using the dynamic Smagorinsky model (Germano *et al.* 1991). Note that in one-way coupled scenarios in which the mass of particles is small compared to the mass of the carrier phase, the computation of the dynamic constant from the Smagorinsky model is completely independent of the calculation of the DF-model parameter b.

When the flow has homogeneous directions, b may be assumed to be independent of such directions. In this way, the condition (2.10) may be enforced on average, which, in the present study, corresponds to a volumetric average represented by the bracketed operator $\langle\cdot\rangle$ below. Specifically, upon substituting $\mathcal{T}_{ij}^{\mathrm{DF}}$ from Eq. (2.9) into Eq. (2.10), the consistency condition becomes

$$\left\langle R_{ij}\overline{S}_{ij}\right\rangle = \left\langle \mathcal{T}_{ij}^{\mathrm{DM}}\overline{S}_{ij}\right\rangle - b^2 \left\langle \overline{S}_{ij}\frac{\partial^2 \mathcal{T}_{ij}^{\mathrm{DF}}}{\partial x_k \partial x_k}\right\rangle, \tag{2.11}$$

with all terms except $\mathcal{T}_{ij}^{\mathrm{DF}}$, which is parameterized by b, being known as functions of the resolved LES velocity field.

Equation (2.11), along with the definitions of G, $\mathcal{T}_{ij}^{\mathrm{DF}}$ and R_{ij} in Eqs. (2.2), (2.7) and (2.8), respectively, correspond to an integral equation in terms of the unknown filter parameter b. This equation must be solved iteratively at each time step, first by guessing a value of b, computing $\mathcal{T}_{ij}^{\mathrm{DF}}$ either by solving Eq. (2.9) or by directly applying the filtering kernel (2.2) to R_{ij}, and then substituting the result in Eq. (2.11) in search of the minimum relative error for b. An alternative approach is to make the approximation

$$\left\langle \overline{S}_{ij}\frac{\partial^2 \mathcal{T}_{ij}^{\mathrm{DF}}}{\partial x_k \partial x_k}\right\rangle \simeq \left\langle \overline{S}_{ij}\frac{\partial^2 \mathcal{T}_{ij}^{\mathrm{DM}}}{\partial x_k \partial x_k}\right\rangle \tag{2.12}$$

in Eq. (2.11). In this approximation, which is used to obtain the results described in Section 3, Eq. (2.11) reduces to the bi-quadratic equation

$$b^4 \left\langle \alpha_{ij}\bar{S}_{ij}\right\rangle + b^2 \left\langle \beta_{ij}\bar{S}_{ij}\right\rangle - \left\langle \mathcal{T}_{ij}^{\mathrm{DM}}\bar{S}_{ij}\right\rangle = 0, \tag{2.13}$$

which can be solved at much lower computational cost, with $b^2 > 0$ corresponding to the relevant root retained in the simulations. In this formulation, the tensor coefficients α_{ij} and β_{ij} are given by

$$\alpha_{ij} = \frac{\partial^2 \overline{u}_i}{\partial x_k \partial x_k}\frac{\partial^2 \overline{u}_j}{\partial x_m \partial x_m}, \tag{2.14}$$

$$\beta_{ij} = 2\frac{\partial \overline{u}_i}{\partial x_\ell}\frac{\partial \overline{u}_j}{\partial x_\ell} + \frac{\partial^2 \mathcal{T}_{ij}^{\mathrm{DF}}}{\partial x_k \partial x_k}. \tag{2.15}$$

Upon obtaining b from Eq. (2.13), the de-filtered velocity u_i computed from Eq. (2.3) is used for time-advancing the particle equation of motion (1.2).

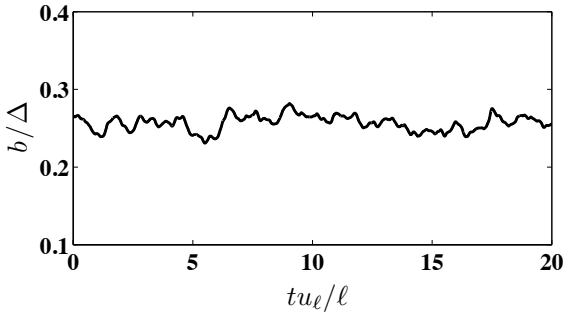

FIGURE 3. Time history of the dynamically determined coefficient b normalized with the LES grid spacing Δ.

3. Model performance

The focus of this section is on examining the performance of the SGS particle model described in the previous section in reproducing preferential-concentration statistics in turbulent flows. Exploration of the model performance in predicting a broader set of disperse-phase statistics is deferred to future work.

3.1. *Computational setup*

The computations involve numerical integrations of Eqs. (1.1)-(1.4) in a triply periodic domain, corresponding to one-way coupled, incompressible homogeneous-isotropic turbulence laden with particles. The Reynolds number based on the Taylor micro-scale is $\mathrm{Re}_\lambda = 85$. The calculations are conducted on staggered, uniform cartesian grids of 256^3 and 32^3 points for DNS and LES, respectively. These grids translate into maximum resolutions $k_{max}\ell_k = 1.5$ and 0.13 for DNS and LES, respectively, where k_{max} is the largest wavenumber resolved by the grid and $\ell_k = (\nu^3/\epsilon_\infty)^{1/4}$ is the Kolmogorov length. The numerical scheme consists of finite-difference discretizations of second-order central in space and fourth-order Runge-Kutta in time (Pouransari *et al.* 2015). Constant-energy linear forcing is applied in the momentum equation (1.4) in order to sustain the turbulence and compute stationary statistics (Bassenne *et al.* 2015). The dynamic constant in the Smagorinsky model is calculated using the least-squares approach of Lilly (1996). A number of particles, which amount to $N_p = 10^7$, are randomly seeded once the flow simulation has reached a statistically steady state. Data collection starts once a sufficiently long time compared to the particle acceleration time t_a has passed after seeding the particles. Time-averaged statistics are extracted from 20 snapshots recorded during $16t_\ell$, with $t_\ell = \ell/u_\ell$ the integral time computed using the associated integral length ℓ and velocity u_ℓ. The characteristic parameter of the simulations is the Stokes number

$$\mathrm{St}_k = t_a/t_k, \tag{3.1}$$

whose values span from 0.1 to 10 in the simulations, with $t_k = \ell_k^2/\nu$ being the Kolmogorov turnover time.

At each time step, the de-filtered velocity u_i computed from the DF model (2.3) is used to integrate the equation of motion for the particles (1.2), with the coefficient b being computed dynamically from Eq. (2.13) according to the dynamic procedure outlined in the previous section. The data shown below include DNS and LES, the latter computed with and without the DF model for particles.

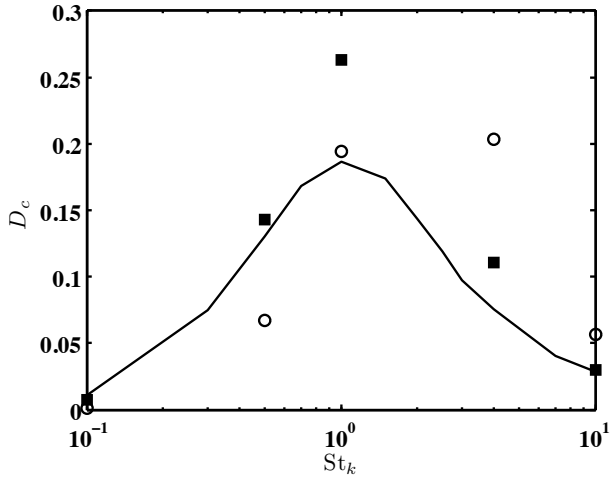

FIGURE 4. D_c-factor for preferential concentration in DNS (solid line), LES with no particle SGS model (circles), and LES with the dynamic DF particle SGS model (squares).

3.2. *Numerical results*

The dynamic computation of the de-filtered velocity u_i is illustrated in Figures 1-3. As mentioned above, the augmentation of the filtered velocity $\overline{u}_i$ by the DF model occurs most intensely near the grid-cutoff scale, as shown in the turbulent-kinetic energy spectra in Figure 1 and in the SGS velocity contours in Figure 2 (right panel). Additionally, Figure 3 shows the time history of the model coefficient b determined with the proposed dynamic procedure based on the consistency in the SGS dissipation. At all simulation time steps, only the positive solution for b^2 in the quadratic equation (2.13) is retained, with no clipping required. Note that the mean value of b resulting from the dynamic procedure, $b/\Delta \approx 0.28$, is in the range $0.16 < b/\Delta < 0.32$, which corresponds to equating the second moment of the differential filter to that of a spherical top-hat filter with a radius in the range $0.5\Delta - 1.0\Delta$.

The computation of particle-laden flows with LES without an SGS particle model generally leads to under- or overprediction of preferential-concentration metrics depending on the value of the Stokes number St_k. The root cause of this underperformance is the deficit of subgrid scales in LES. Specifically, the minimum fluctuation time scale of the turbulence is increased from the Kolmogorov time t_k in DNS to the grid-cutoff time $t_\Delta \sim (\Delta/\ell_k)^{2/3} t_k$ in LES. As a result, in LES without an SGS particle model the effective Stokes number is closer to $\mathrm{St}_{\mathrm{SGS}}$ than to St_k, with $\mathrm{St}_{\mathrm{SGS}} < \mathrm{St}_k$ given in Eq. (1.5), and preferential concentration tends to be overpredicted for $\mathrm{St}_k > 1$ an underpredicted for $\mathrm{St}_k < 1$. These erroneous dynamics can be palliated using the dynamic DF model, as shown below.

Preferential-concentration statistics are presented in Figure 4 in terms of the global factor

$$D_c = \sum_{C=0}^{N_p} \left[p_c(C) - P_c(C) \right]^2 , \tag{3.2}$$

where $p_c(C)$ is the fraction of computational cells containing C particles, and $P_c(C)$ is the discrete Poisson probability density function. Positive deviations from the random

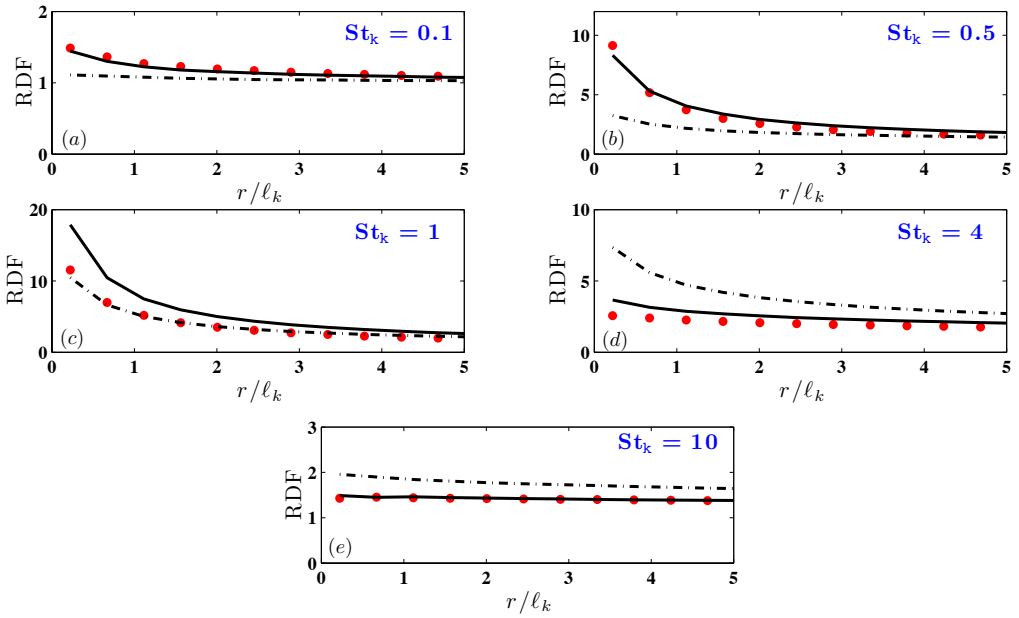

FIGURE 5. Radial distribution functions (RDF) as functions of the radial distance in DNS (circles). LES with no particle SGS model (dashed lines), and LES with the dynamic DF particle SGS model (solid lines).

distribution $D_c = 0$ depicted in Figure 4 represent departures from a random distribution of particle concentration and are therefore ascribed to preferential concentration of particles (Squires & Eaton 1991), which becomes maximum at Stokes numbers $\mathrm{St}_k \sim 1$ in homogeneous-isotropic turbulence. Although the non-monotonic trend of D_c is clearly captured by DNS, it is missed by LES when no SGS model for particles is employed. In contrast, prediction of the D_c factor for $\mathrm{St}_k < 1$ and $\mathrm{St}_k > 1$, along with its non-monotonic trend, improves considerably when the dynamic DF model is used, except for $\mathrm{St}_k \sim 1$ for which LES without an SGS model for particles performs better.

Similar conclusions are drawn from analysis of the radial distribution functions (RDF) in Figure 5, which quantify the likelihood of any pair of particles being separated at a distance r (e.g., see Ray & Collins (2011) for further details on the use of RDF for particle-laden flows), and from analysis of the particle-concentration spectra in Figure 6, the latter computed by projecting the Lagrangian particles from the DNS and the LES on the same Eulerian grid with 128^3 grid points. In particular, the recovery of preferential-concentration statistics from DNS by using LES with the dynamic DF model is remarkable for $\mathrm{St}_k < 1$ and $\mathrm{St}_k > 1$ in the RDFs and in the energetic part of the concentration spectra. The underperformance of the dynamic DF model at $\mathrm{St}_k \sim 1$ is the subject of current investigation.

It should be stressed here that, in contrast to the dynamic DF model presented in this study, traditional stochastic models are unable to predict the non-monotonicity of the preferential-concentration metrics shown in Figures 4-6 (Minier 2015). In particular, stochastic models tend to disperse the particle distribution by injecting random amounts of flow velocity in Eq. (1.2) in order to reproduce the effect of the SGS velocity fluctuations, which in this study are modeled using Eq. (2.8) instead. As a consequence, stochastic models perform correctly for $\mathrm{St}_k > 1$, in that they decrease the preferential

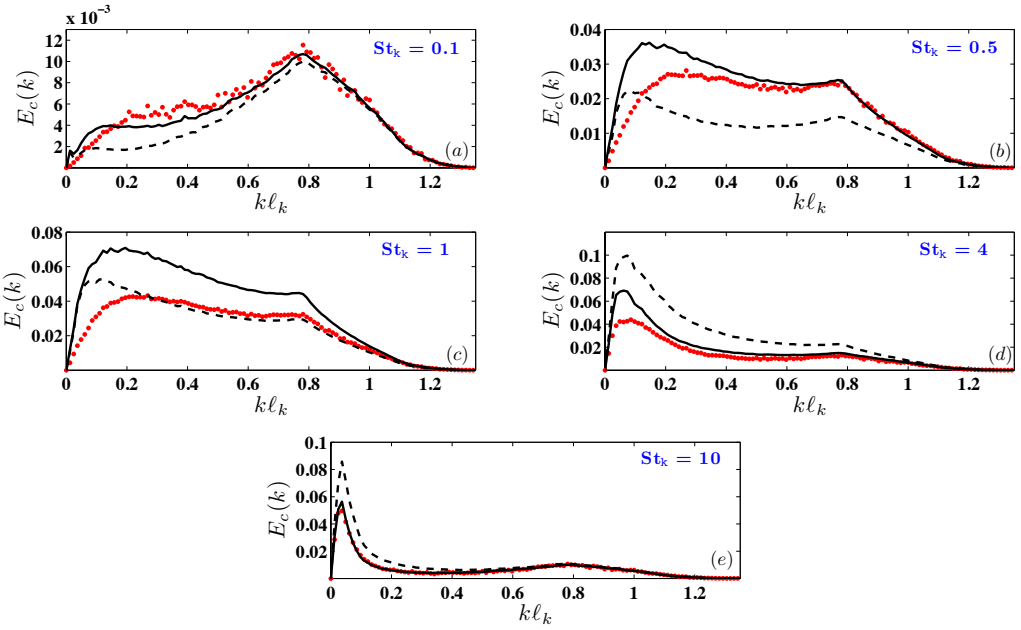

FIGURE 6. Particle-concentration spectra as functions of the wavenumber k in DNS (circles). LES with no particle SGS model (dashed lines), and LES with the dynamic DF particle SGS model (solid lines).

concentration level that would otherwise be artificially high if LES with no SGS particle model were used. However, they underperform in describing preferential concentration for $\mathrm{St}_k < 1$, for which anti-dispersion, rather than dispersion, is required from the SGS particle model.

4. Conclusions and future plans

A new dynamic particle SGS model based on elliptic differential filters is proposed in this study. The proposed model, referred to as dynamic DF, computes the full-scale velocity required for integration of the particle equation of motion by de-filtering the resolved LES velocity field with a differential filter. The model parameter b, which is related to the nominal filter width, is determined dynamically by imposing consistency between the SGS dissipations predicted by the dynamic DF model and by the LES model used to integrate the carrier-phase conservation equations. The resulting model is simple, involves no significant computational overhead, contains no adjustable parameters, and can be deployed in any type of flow solvers and grids, including unstructured setups.

The proposed model is tested in homogeneous-isotropic turbulence laden with particles. The results show that, except for near-unity Stokes numbers, the dynamic DF model captures to a remarkable degree the preferential concentration statistics predicted by DNS and significantly improves predictions over LES computations that are not supplied with any SGS particle model. Specifically, the dynamic DF model is capable of reproducing the non-monotonicity of the preferential concentration statistics with respect to the Stokes number, a characteristic rarely achieved in stochastic models. Future work will involve

further improvements, including predictions at near-unity Stokes numbers along with model extensions to non-isothermal and wall-bounded flows.

Acknowledgments

This investigation was funded by the Advanced Simulation and Computing (ASC) program of the US Department of Energy's National Nuclear Security Administration via the PSAAP-II Center at Stanford.

REFERENCES

Bassenne, M., Urzay, J., Park, G. I. & Moin, P. 2015 Constant-energetics physical-space forcing methods for improved convergence to homogeneous-isotropic turbulence with application to particle-laden flows. Submitted to *Phys. Fluids*.

Okong'o, N. & Bellan, J. 2000 A priori subgrid analysis of temporal mixing layers with evaporating droplets. *Phys. Fluids* **12**, 1573–1591.

Jiménez, J. & Moser, R. D. 2000 Large-eddy simulations: Where are we and what can we expect? *AIAA J.* **38**, 605–612.

Germano, M. 1986a Differential filters for the large-eddy numerical simulation of turbulent flows. *Phys. Fluids* **29**, 1755–1757.

Germano, M. 1986b Differential filters of elliptic type. *Phys. Fluids* **29**, 1757–1758.

Germano, M., Piomelli, U., Moin, P. & Cabot, W. H. 1991 A dynamic subgrid-scale eddy viscosity model. *Phys. Fluids* **3**, 1760–1765.

Lilly, D. K. 1996 A proposed modification of the Germano subgridscale closure method. *Phys. Fluids* **4**, 633–635.

Minier, J. P. 2015 On Lagrangian stochastic methods for turbulent polydisperse two-phase reactive flows. *Prog. Energy Comb. Sci.* **50**, 1–62.

Pouransari, H., Mortazavi, M. & Mani, A. 2015 Parallel variable-density particle-laden turbulence simulation. *Annual Research Briefs*, Center for Turbulence Research, Stanford University, pp. 43-54.

Ray, B. & Collins, L. R. 2011 Preferential concentration and relative velocity statistics of inertial particles in Navier-Stokes turbulence with and without filtering. *J. Fluid Mech.* **680**, 488–510.

Sánchez, A. L., Urzay, J. & Liñán, A. 2014 The role of separation of scales in the description of spray combustion. *Proc. Combust. Inst.* **35**, 1549–1577.

Squires, K.D. & Eaton, J.K. 1991 Preferential concentration of particles by turbulence. *Phys. Fluids. A* **3.5**, 1169-1178.

Urzay, J., Bassenne, M., Park, G. I. & Moin, P. 2014 Characteristic regimes of subgrid-scale coupling in LES of particle-laden turbulent flows. *Annual Research Briefs,* Center for Turbulence Research, Stanford University, pp. 3–13.